

# Pushing Back Studies of Galaxies Toward the Dark Ages: High-Redshift Ly $\alpha$ Emission-Line Galaxies in the Field

Esther M. Hu

*Institute for Astronomy, University of Hawaii, 2680 Woodlawn Drive,  
Honolulu, HI 96822, USA*

**Abstract.** Ly $\alpha$  emission presents a means of identifying very high redshift galaxies, provided such objects can be reliably distinguished from foreground emission-line galaxies. Here we report on a program of imaging and spectroscopic studies being conducted with the Keck telescope, in concert with additional efforts from the ground and with HST, to study such high-redshift objects over the range from  $z = 3 \rightarrow 7$ . The first deep narrow-band imaging studies with Keck are used to show that strong Ly $\alpha$  emitters, such as have been seen in high-redshift quasar fields at  $z > 4.5$ , can be found in the field populations. Based on studies of the HDF and the Hawaii Survey Fields these are significant contributors to the star formation rates at these epochs.

## 1. Introduction

Recent attempts to identify and study galaxies at the high end of the currently known redshift range ( $z \sim 4 \rightarrow 5$ ) have primarily focused on color-selection techniques, which rely on the strong depression of the continuum below the redshifted Lyman break to roughly select out candidates by redshift. This method, suggested by Cowie (1988) and so successfully applied by Steidel and co-workers (1996) to galaxies up to redshifts of 3.5, has been recently extended to  $z \sim 4.92$  by Franx et al. (1997) in the case of gravitationally lensed objects.

However, the first objects found at  $z > 4$  were seen to have strong Ly $\alpha$  emission, and could be selected by this property. In the case of BR1202-0725e, the close companion to a  $z = 4.69$  quasar, both Ly $\alpha$  emission (Hu et al. 1996, Petitjean et al. 1996) and color selection (Fontana et al. 1996) were capable of distinguishing the source as a high-redshift object. However, other high- $z$  Ly $\alpha$  emitters found in quasar fields, but well-separated from the quasars, were found with extremely weak continua, and could not have been found by color-selection methods (Hu & McMahon 1996). This suggests that these populations may also be prevalent in the field samples.

The Lyman alpha searches are complementary to the color techniques for two reasons. First, at higher redshifts ( $z > 5$ ), (unlensed) continuum magnitudes become very faint, and the identification and spectroscopic confirmation of color-selected galaxies becomes progressively more difficult. Here direct selection of Ly $\alpha$  emitters represents our best chance of finding and mapping a large sample of high- $z$  galaxies. Secondly, even at more moderate redshifts ( $z = 2 \rightarrow 4$ ) where such objects have been seen (e.g., Pascarelle et al. 1996), the Ly $\alpha$  emitters may

represent earlier and less reddened stages in the galaxy formation process, and measured luminosities, sizes, velocity widths and clustering as a function of the line's equivalent width may provide crucial insights into very early galaxy growth.

The present paper reports on an ongoing program to study very high redshift galaxies selected by their Ly $\alpha$  emission properties, and also demonstrates the first use of narrow-band filters on the new large (8-  $\rightarrow$  10-m class) telescopes. Such objects are significant contributors to the integrated star formation in the field galaxy population by redshifts  $z \sim 3.4$  (Cowie & Hu 1998).

## 2. Narrow-band imaging searches at $z = 3 \rightarrow 5$

As a first step in investigating high- $z$  emitters in the field, we undertook narrow-band searches of well-studied fields in the HDF and Hawaii Galaxy Surveys. The extensive deep, multi-color imaging and spectroscopic coverage of these fields from the ground and with *HST* make them ideal testbeds for: (1) comparing methodologies and sensitivities of emission-line vs continuum color-break techniques for identifying high-redshift galaxies, (2) determining relative numbers of foreground emission-line objects and determining the best methods for distinguishing between (Ly $\alpha$ , [O II], H $\beta$ , [O III]) emitters, (3) estimating the relative surface density of high-redshift candidates as a function of flux from each technique, and (4) establishing a baseline for comparing blank-field and targeted searches around high- $z$  objects (such as radio galaxies, DLAs, and quasars), and for the evolution of galaxy properties at higher redshifts. Such studies then permit fine-tuning the search procedures. Two filters, corresponding to Ly $\alpha$  at  $z \sim 3.4$  and 4.6, were chosen to begin these studies in redshift ranges overlapping color studies in the literature and by our collaborators (Giallongo et al. 1997).

In Fig. 1 we show a 2-hour exposure on the Hubble Deep Field (HDF) obtained using the 5390 Å (77 Å wide) filter on LRIS. The narrow-band image is compared with an ultra-deep *V*-band image which was also obtained on LRIS, and covers an area of  $380'' \times 275''$ , with FWHM of  $\sim 0.7''$  and a  $1 \sigma$  limiting narrow-band magnitude of  $N(AB)=26.8$  in a  $3''$  diameter aperture, corresponding to a  $1 \sigma$  flux limit of  $6 \times 10^{-18}$  erg cm $^{-2}$  s $^{-1}$ .

There are 719 objects in the field above the  $5 \sigma$  limit, of which 222 have redshifts in the literature. Five of the objects in the HDF narrow-band sample have observed equivalent widths in excess of 100 Å and are circled in Figure 1. This selection immediately recovers the one known object lying within the redshift interval, the  $z = 3.430$  object hd2-06980-1297 (shown in heavy circle), which was identified by Lowenthal et al. (1997) based on emission and absorption lines in an LRIS spectrum.

Of the eleven objects with equivalent widths in excess of 100 Å identified in this way in the HDF and SSA22, two are completely absent in the continuum *B*, *V*, *R*, *I*, *J*, *K* images ( $V > 27$ ) and have observed equivalent widths in excess of 500 Å, but the remainder have colors which would place them at high redshift. In Fig. 2 we plot the locus of colors for the narrow-band selected objects in the two fields. The objects that meet our equivalent width criterion (*solid squares*) have predominantly red ( $B - V$ ) colors, but are blue (or close to flat-spectrum  $f_\nu$ ) in ( $V - I$ ) colors, as would be expected for high-redshift objects that are dominated

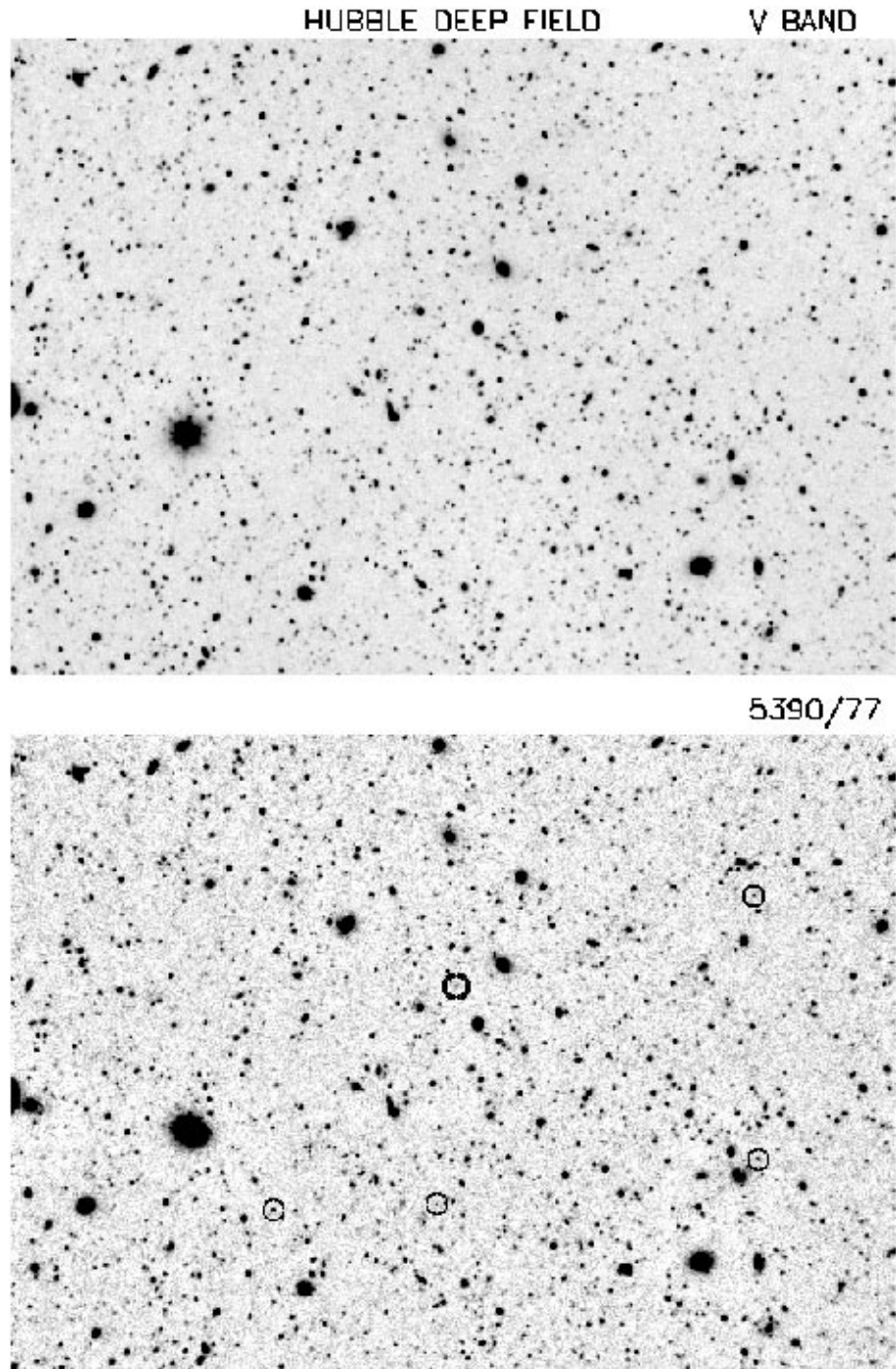


Figure 1. Deep Keck LRIS images of the HDF in  $V$  (*top*) and through a narrow-band filter centered at  $5390 \text{ \AA}$  (*bottom*). Circles show strong emitters, which are candidate  $\text{Ly}\alpha$  galaxies. This recovers the one object (*heavy circle*,  $z = 3.430$ ) with known  $\text{Ly}\alpha$  in the filter bandpass.

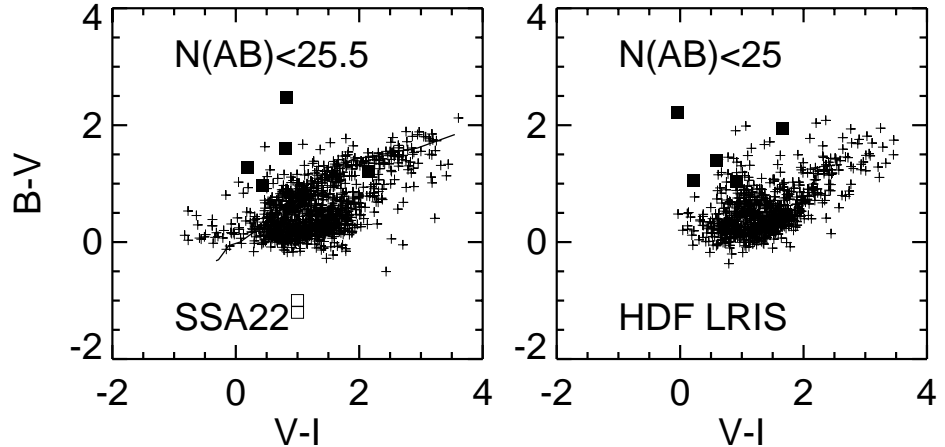


Figure 2.  $(B - V)$  vs  $(V - I)$  color-color plots for objects in the HDF and SSA22 fields selected from the narrow-band catalogues ( $N(AB) < 25$  for the LRIS HDF field and  $N(AB) < 25.5$  for the LRIS SSA22 field). The colors of emission-line objects in these magnitude-selected catalogues with equivalent widths in excess of  $100 \text{ \AA}$  in the observed frame are indicated with squares, and lie at red ( $B - V$ ) and blue ( $V - I$ ) colors. Two of the strong emission-line objects in the SSA22 field have continua which are either undetected or too faint to provide color measurements. They are indicated schematically by open squares placed at nominal color positions.

by star formation (Cowie 1988, Steidel et al. 1996, Lowenthal et al. 1997) and which have strong Lyman alpha forest absorption in the  $B$  band. These objects occupy the same region of the color-color diagram as objects seen in the tail of the color-color distribution for the HDF proper, and which correspond to spectroscopically identified high-redshift galaxies selected by color.

The objects which are not detected in the continuum lie in the SSA22 field. Because the equivalent widths in these objects are so high, the lines are unlikely a priori to be  $[\text{O II}]$  or  $[\text{O III}]$ , where rest equivalent widths generally do not exceed  $100 \text{ \AA}$ . However, in order to check this further, we obtained spectra of the objects in August of this year using the LRIS spectrograph in the multi-object mode. The spectra of the two objects are shown in Fig. 3 where we compare them with the highest equivalent width  $[\text{O II}]$  line emitter found in the Hawaii spectrographic surveys. The  $[\text{O II}]$  galaxy, which is characteristic of all the spectra with high  $[\text{O II}]$  equivalent widths (cf., Fig. 4), has extremely strong  $[\text{O III}]$  and  $\text{H}\beta$ , which are features not present in the candidate  $\text{Ly}\alpha$  emitters. Similarly, the more unlikely possibility that the line is  $[\text{O III}]$  is ruled out by the absence of the  $\text{H}\alpha$  line and the  $[\text{O III}]$  and  $\text{H}\beta$  complex. There therefore appears little doubt that these objects are indeed  $\text{Ly}\alpha$  emitters. We may also note the the absence of strong  $\text{C IV}$  in the spectra.

The extensive redshift information which is available for the fields also allows us to check the equivalent width selection procedure. In Fig. 5 we show  $(V - N)$  vs. redshift, with the redshift intervals matching the narrow-band filter band-pass indicated for emission from  $[\text{O III}] \lambda 5007$  (at  $z \sim 0.08$ ),  $[\text{O II}] \lambda 3727$

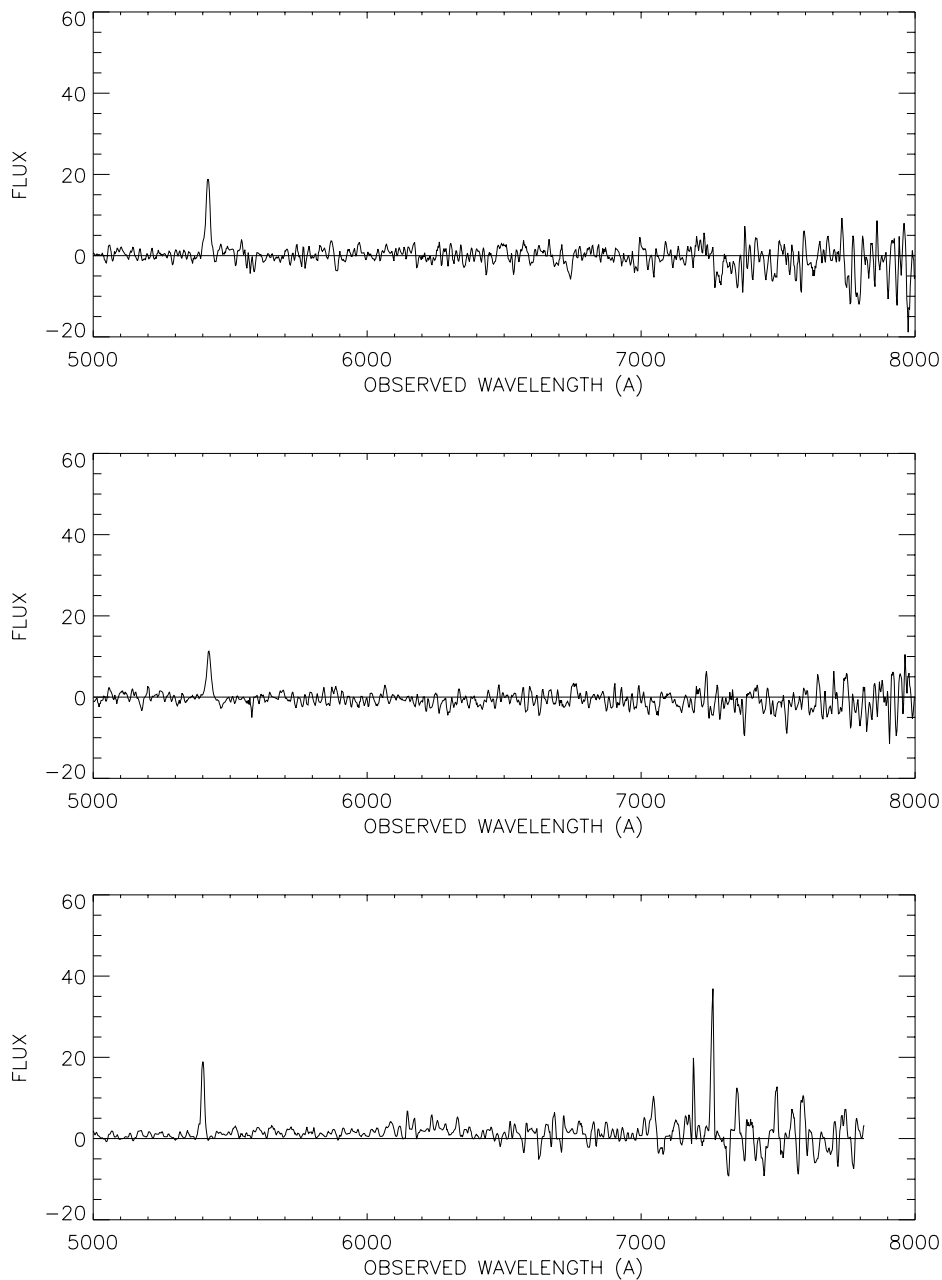


Figure 3. Spectra of SSA22 strong Ly $\alpha$  emitters without detected  $V$  continua (*top two panels*) compared with the spectrum of an [O II] emitter with extremely high equivalent width (*bottom panel*) shifted so the [O II] emission lies at the narrow-band wavelength. The H $\beta$  and [O III] complex is clearly evident in the case of the [O II] emitter, and these cases may be easily distinguished from genuine high- $z$  Ly $\alpha$  emission objects.

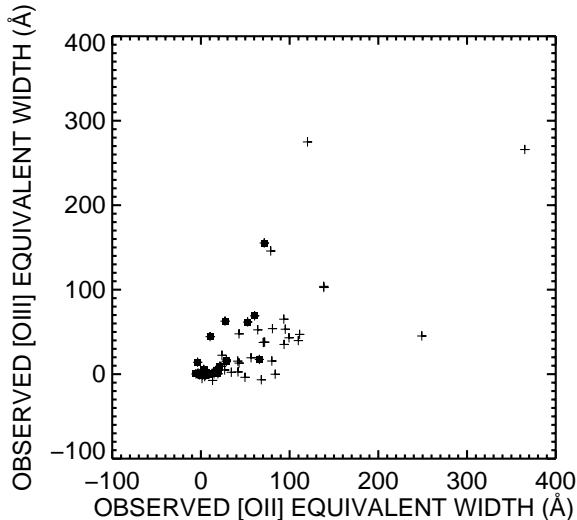


Figure 4. Plot of [O III] vs [O II] equivalent widths (*pluses*) from the magnitude-selected Hawaii Survey Fields. Overplotted points (*solid boxes*) show the  $z < 0.5$  emitters.

(at  $z \sim 0.45$ ), Mg II  $\lambda$  2800 (at  $z \sim 0.93$ ), and Ly $\alpha$   $\lambda$  1216 (at  $z \sim 3.43$ ). These are the most prominent spectral features in most galaxies, with Mg II normally seen in absorption, and they are clearly seen in the color-redshift plot. The scatter of points gives an idea of the real distribution of the signal strength of each feature, and it may also be seen that the high- $z$  Ly $\alpha$  emitter, corresponding to the Lowenthal et al. object, does indeed have appreciably higher equivalent width than any of the [O II] emitters, though it is in fact one of the lowest equivalent width objects in the sample. Other structures arise from additional spectral features (*e.g.*, the 4000 Å break and [Fe II] absorption lines), which add to the dispersion.

As we move to higher redshift ( $z = 4.6$ ) we continue to see high equivalent emitters ( $W > 100$  Å in the observed frame). A 2-hr exposure taken through the 6740/80 Å narrow-band filter produced 3 such objects with  $AB < 24.5$ . The lowest equivalent width object is an [O II] emitter which has a strong [O III] and H $\beta$  complex, while the two higher equivalent width objects are Ly $\alpha$  emitters. In the spectroscopic studies, probable [O II] emitters are also targeted for followup spectra, in order to understand the differences between emission-line selection and continuum selection. This will be particularly important to make a convincing case for objects where the corresponding [O II] line cannot be detected (*e.g.*, at  $z \gtrsim 5.2$ ), in contrast to the case for the  $z = 4.5 \rightarrow 4.7$  Ly $\alpha$  emitters (*cf.*, Hu et al. 1997; Egami 1998).

In the three fields that we have observed so far there are approximately six Ly $\alpha$  emitters per 23  $\square'$  field or about 1,000/ $\square^\circ$  lying in the redshift range  $z = 3.405 \rightarrow 3.470$ , or roughly 15,000/unit  $z/\square^\circ$ . Most of the objects detected in the continuum have  $V < 25.25$ . To this  $V = 25.25$  magnitude limit a color criterion  $(B - V) > 1$ ,  $(V - I) < 1.6$  of the type discussed above gives 80 objects per sample area, or assuming a  $z$  range of  $3.1 \rightarrow 3.5$ , where the upper limits is

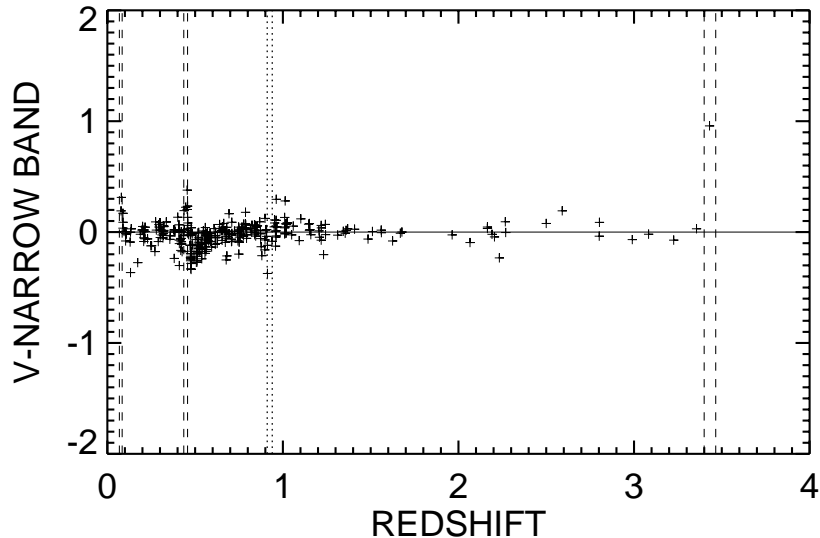


Figure 5. Excess emission in narrow-band over  $V$ -band vs redshift from objects in the HDF and SSA22 fields. Objects with spectroscopic identifications in the literature over the HDF and SSA22 fields sampled by the LRIS deep imaging fields are shown here. The positions and redshift ranges corresponding to features such as  $\text{Mg II}$  (*dotted lines*) and  $[\text{O III}]$ ,  $[\text{O II}]$ , and  $\text{Ly}\alpha$  (*dashed lines*) falling within the filter bandpass are indicated. The structure of the continuum near the  $[\text{O II}]$  feature may be seen reflected in both the ‘dip’ and dispersion of points in this region, and it may also be seen that emission-line objects in  $[\text{O II}]$  and a few  $[\text{O III}]$  emitters may be detected. Underlying continuum features can also increase the dispersion of points in different redshift regions.

determined by the passage of the forest through the red edge of the  $V$  band, a surface density of 15,000/unit  $z/\square^\circ$ . While the number is quite uncertain because of the small number statistics, the choice of magnitude cutoff and the possibility of redshift clustering, a large fraction – very roughly half – of the  $B$  drop-out galaxies are strong  $\text{Ly}\alpha$  emitters. This is roughly consistent with the Lyman alpha emitting fraction of the color selected galaxies with measured high redshifts, again giving us confidence that the methodology is sound.

The rest frame equivalent widths of the systems are consistent with stellar excitation for an initial mass function dominated by massive stars (Charlot & Fall 1993). If the observed emission were primarily due to stars, and there were no internal scattering and extinction, then a luminosity of  $10^{42}$  erg  $\text{s}^{-1}$  would correspond to a star formation rate in solar masses ( $M_\odot$ ) per year of  $\sim 1 M_\odot \text{yr}^{-1}$ , where we use Kennicutt’s (1983) relation between  $\text{H}\alpha$  luminosity and star formation rate (SFR) of  $\text{SFR} = L(\text{H}\alpha) \times 8.9 \times 10^{-42} \text{ erg s}^{-1} M_\odot \text{yr}^{-1}$ , and assume a ratio of  $\text{Ly}\alpha$  to  $\text{H}\alpha$  (8.7) that applies for Case B recombination. Given the Hubble time at these redshifts of  $7 \times 10^8 h^{-1} \text{ yr}$  ( $q_0 = 0.5$  for  $z = 4.6$ ) the integrated amount of star formation in the objects is clearly small compared to that of a ‘normal’  $L^*$  galaxy with  $6 \times 10^{10} h^{-1} M_\odot$  of stars.

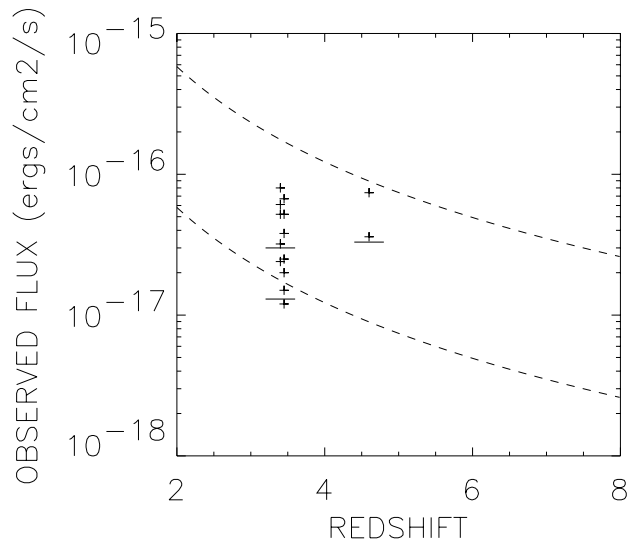


Figure 6. Crosses show the line fluxes of the objects at  $z = 3.4$  in three fields and at  $z = 4.6$  in the SSA22 field only. The solid lines show the 5 sigma detection limits for bare line emitters for the 2-hour exposure at  $5390 \text{ \AA}$  in the HDF and the 5-hour exposure in the SSA22 field and the 2-hour exposure at  $6740 \text{ \AA}$  in the SSA22 field. (Some objects lie slightly below these limits because of the continuum subtraction.) There is relatively little wavelength dependence in the sensitivity limit at the same exposure time because the filters have been positioned in relatively line free regions of the night sky. The dashed lines show the expected fluxes for objects with  $1 \times 10^{42} \text{ erg s}^{-1}$  and  $1 \times 10^{43} \text{ erg s}^{-1}$  for  $H_0 = 65 \text{ km s}^{-1} \text{ Mpc}^{-1}$  and  $q_0 = 0.5$ . For dust-free objects with Salpeter mass functions these Ly $\alpha$  luminosities correspond to 1 and 10  $M_\odot$  per year respectively.

### 3. Next steps

The next stage in the project is to develop much larger samples at the two redshifts already covered by the prototyping project and to extend the work into the  $z > 5$  range using longer wavelength filters. Figure 6 provides an overview of what we require in both these areas by showing the line fluxes of the existing objects at the two redshifts together with the sensitivity limits and the expected decrease in the fluxes as a function of redshift for  $q_0 = 0.5$  models. These data will be combined with ongoing deep multi-color optical/IR studies for both field samples and high- $z$  quasar fields (in upcoming HST observations),

Searches for yet higher  $z$  galaxies are of necessity forced into the near IR since the light below  $1216(1+z) \text{ \AA}$  will be essentially extinguished by the strong Ly  $\alpha$  forest blanketing or by H I Gunn-Peterson at the redshifts where the IGM was neutral. Objects at these high redshifts will also be extremely faint: even for  $q_0 = 0.5$  a galaxy burning  $10^{10} M_\odot$  of baryons in a Hubble time with a Salpeter IMF will have an  $AB$  magnitude of roughly 26.5 (100 nJy) — almost

irrespective of redshift — at wavelengths corresponding to the rest ultraviolet ( $1216 \text{ \AA} - 300 \text{ \AA} (1 + z)$ ) (e.g., Cowie 1988). For  $q_0 = 0$  the result is redshift dependent, but such a galaxy at  $z = 8$  would be almost an order of magnitude fainter. Impulsive burning could increase the flux a little but probably not by more than an order of magnitude even in the open case. Since characteristic baryon masses in these early objects are likely to be about  $10^8 - 10^9 M_\odot$  we will probably have to reach nJy level fluxes to detect populations at these redshifts. We can look forward to detecting these objects with NGST.

**Acknowledgments.** This work was supported in part by NASA grants GO-6222.01-95A and AR-6377.06-94A from Space Telescope Science Institute, which is operated by AURA, Inc. under NASA contract.

## References

- Charlot, S. & Fall, S. M. 1993, ApJ, 415, 580
- Cowie, L. L. 1988, in *The Post-Recombination Universe*, ed. N. Kaiser & A. Lazenby (Dordrecht: Kluwer), 1
- Cowie, L. L. & Hu, E. M. 1998, AJ, in press [astro-ph/9801003]
- Cowie, L. L., Songaila, A., Hu, E. M., & Cohen, J. G. 1996, AJ, 112, 839
- Egami, E. 1998, to appear in *The Ultraviolet Universe at Low and High Redshift*, ed. W. H. Waller, M. N. Fanelli, J. E. Hollis, & A. C. Danks (New York: AIP Press)
- Fontana, A., Cristiani, S., D’Odorico, S., Giallongo, E. & Savaglio, S. 1996, MNRAS, 279, L27
- Franx, M., Illingworth, G. D., Kelson, D. D., van Dokkum, P. G., & Tran, K.-V. 1997, ApJ, 486, L75
- Giallongo, E., D’Odorico, S., Fontana, A., Cristiani, S., Egami, E., Hu, E. M., & McMahon, R. G. 1997, AJ, submitted
- Hu, E. M., & McMahon, R. G. 1996, Nature, 382, 231
- Hu, E. M., McMahon, R. G., & Egami, E. 1996, ApJ, 459, L53
- Hu, E. M., McMahon, R. G., & Egami, E. 1997, in *HST and the High Redshift Universe*, ed. N. Tanvir, A. Aragón-Salamanca, & J. Wall (Singapore: World Scientific), p. 91
- Kennicutt, Jr., R. C. 1983, ApJ, 272, 54
- Lowenthal, J. D. *et al.* 1997, ApJ, 481, 673
- Pascarelle, S. M., Windhorst, R. A., Keel, W. C. & Odewahn, S. C. 1996, Nature, 383, 45
- Petitjean, P., Pécontal, E., Valls-Gabaud, D. & Charlot, S. 1996, Nature, 380, 411
- Steidel, C. C., Giavalisco, M., Pettini, M., Dickinson, M., & Adelberger, K. L. 1996, ApJ, 462, L17
- Williams, R. E. *et al.* 1996, AJ, 112, 1335